Materials Science and Engineering A 400–401 (2005) 125–131

MATERIALS SCIENCE & ENGINEERING A

www.elsevier.com/locate/msea

Gradients of geometrically necessary dislocations from white beam microdiffraction

R.I. Barabash*, G.E. Ice, J.W.L. Pang

Metals and Ceramics and Solid State Divisions, Oak Ridge National Laboratory, Oak Ridge, TN 37831-6118, USA

Received 13 September 2004; received in revised form 3 January 2005; accepted 28 March 2005

Abstract

Variations in the local crystallographic orientation due to the presence of geometrically necessary dislocations and dislocation boundaries smear the distribution of intensity near Laue reflections. Here, some simple model distributions of geometrically necessary dislocations, GNDs, are used to estimate the dislocation tensor field from the intensity distribution of Laue peaks. Streaking of the Laue spots is found to be quantitatively and qualitatively distinct depending on the ratio between the absorption coefficient and the GND density gradient. In addition, different slip systems cause distinctly different Laue-pattern streaking. Experimental Laue patterns are therefore sensitive to stored dislocations and GNDs. As an example, white beam microdiffraction was applied to characterize the dislocation arrangement in a deformed polycrystalline Ni grain during in situ uniaxial tension.
© 2005 Elsevier B.V. All rights reserved.

Keywords: X-ray diffraction; Strain gradient; Synchrotron radiation; Dislocations

1. Introduction

Nondestructive probes covering a range of spatial resolutions, momentum transfer resolutions and penetration depths have recently been developed for the analysis of structure evolution in materials [1–4]. For studies of inhomogeneous deformation, white beam probes [3,4] have unique advantages: (1) the sample does not need to be rotated which allows for good spatial resolution; (2) the intensity distributions around a large number of different reflections can be simultaneously analyzed from the same subgrain; (3) an uncompromised full three-dimensional (3D) reciprocal space intensity distribution can be measured when necessary by scanning the incident beam energy; and (4) the local environment can be characterized near a volume element of interest.

With white beam microdiffraction it is also possible to quantitatively analyze a sample at different structure levels. In particular, it is now possible to analyze details of structure corresponding to nano (cells) and mesoscopic (fragments) levels. For example, at small strains, geometrically necessary boundaries (GNBs) are composed of dense dislocation walls (DDWs) or double walled microbands (MB) inclined in the direction of metal flow. At large strains they can form almost parallel lamellar bands (LB) [5–15]. These micro bands are distinguishable mainly due to the differences in local orientation as well as morphology differences of the dislocation structure within the deformation microbands [6]. Large cumulative misorientation within one grain was recently observed by 3D XRD [14]. Large intensity gradients have also been observed in the Laue signature of some experiments [16–18].

Gradients in cell-wall structure arise from plastic strain gradients that can be detected through inhomogeneous lattice rotations along the probe direction. This inhomogeneous behavior can lead to asymmetric Laue spots or to other intensity variations along the Laue streak; the actual intensity distribution depends on the dislocation density distribution. Here, we describe how the dislocation tensor field can be estimated from the shape of Laue spots collected with polychromatic X-ray microdiffraction. An example is presented to illustrate the application to a real sample.

* Corresponding author. Tel.: +1 865 2417230; fax: +1 865 5747659.
E-mail address: barabashr@ornl.gov (R.I. Barabash).

0921-5093/$ – see front matter © 2005 Elsevier B.V. All rights reserved.
doi:10.1016/j.msea.2005.03.036

2. Experimental details

Measurements were made on the 3D X-ray crystal microscope of beamline 34-ID at the Advanced Photon Source, Argonne I1. The 3D X-ray crystal microscope uses a modified Laue diffraction method based on polychromatic radiation [3,4]. This approach allows for true 3D mapping of crystalline phase, orientation, elastic strain and plastic deformation with unprecedented submicron spatial resolution. In particular, differential-aperture microscopy [4] resolves the local crystallographic structure along the path of the incident X-ray microbeam. This allows for detailed 3D mapping of the local crystallographic structure in materials. As described in ref. [4], the depth-dependent intensity contributions to all pixels of the detector are reconstructed from the variation in the CCD pattern as a wire passes near the sample surface. Details on the experimental setting and data collection can be found elsewhere [4].

In this experiment, rotations of five neighboring grains in a polycrystalline Ni tensile sample were determined at three levels of strain. Here, we present the results for one grain at 15% plastic strain. Dimensions of the beam were 0.5 μm × 0.5 μm with a penetration depth of ∼30 μm. Rotations were resolved with ∼1 μm resolution along the incident beam [3,4].

Under some conditions of plastic deformation, large dislocation density gradients are observed even within the micrometre-scale resolved volume element along the incident beam direction. In these cases, intensive streaking is observed even from the Laue patterns within the differentially resolved volumes. In order to get additional information about the plastic strain gradients within these highly deformed volume elements, the results of standard differential aperture microscopy (DAXM) are extended with a Laue intensity analysis of local streaking. Samples requiring this kind of analysis include highly deformed samples, thin film structures or materials with a very high absorption coefficient (e.g., Ir); in these samples the strain gradients are either too high or the small range of sampling along the beam direction prevents standard DAXM analysis.

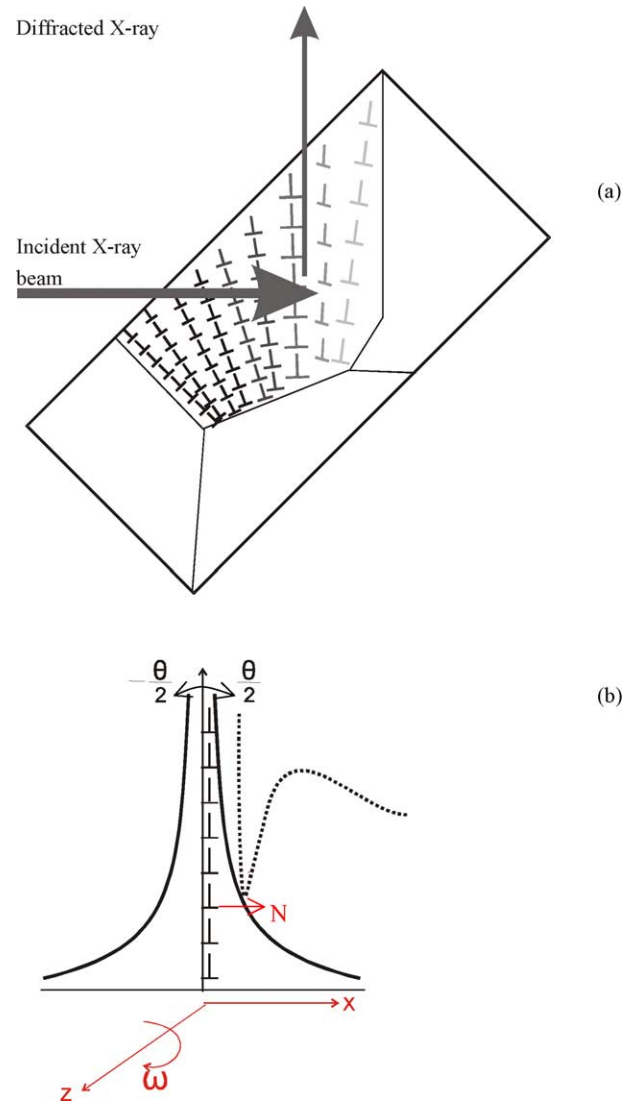

Fig. 1. (a) Cell-wall structure with decaying density of dislocation walls within the depth of the grain, (b) shielding of stress fields σ due to grouping of dislocations within infinite equidistant dislocation walls; axis X is perpendicular to the plane of the wall, axis Z is parallel to the rotation axis; axes Y and Z are in the plane of the wall. Solid curve shows the decay of long-range strain and stress fields σ with the distance x from the infinite dislocation wall and a tendency for long-range strain to reappear near the finite equidistant dislocation wall [19] or near the wall with irregular dislocation positions (dashed curve).

3. Models of cell-wall substructure with varying dislocation density

3.1. Parameters of cell-wall structure

Consider deformation cells with distinct orientations separated by geometrically necessary boundaries formed by tilt dislocation walls as shown in Fig. 1a. Each wall provides a rotation between neighboring cell blocks around the direction of the dislocation lines within the wall. The unit vector $\boldsymbol{\omega}$ parallel to the rotation axis of each wall coincides with the unit vector $\boldsymbol{\tau}$ along the dislocation lines in the case of a tilt boundary. We consider tilt dislocation walls formed by equidistant edge dislocations with Burgers vector $\boldsymbol{b}$ (so called "thin walls" [5–10]). Long-range internal strains from individual dislocations within the infinite "thin" wall shield each other (Fig. 1b). As a result "thin" walls inhibit long-range strain while allowing rotations between cell blocks.

The misorientation angle Θ due to such a boundary is defined by the equation $b/h = 2\sin(\Theta/2)$, where $b/h \approx \Theta$ for small angle boundary. If h is the distance between these dislocations in the wall, one can consider the boundary as a single defect producing a local rotation field. According to Saada and Bouchaud [19], walls made of a finite number of parallel dislocations cause long-range interactions in the cell interior

to reappear. However, with increasing length of the walls, this input becomes smaller and their displacement fields can be treated as an infinite thin wall to a first approximation.

We define the average size of the deformation cell D^+ between the two nearest GNBs and write the linear density of GNBs as the number of walls per unit length, $1/D^+$. The total density of unpaired dislocations grouped in the walls is denoted by $n^+ = \frac{1}{D^+ h}$. We use a Cartesian coordinate system with axis Z parallel to the direction of dislocation lines within the wall and axis X perpendicular to the plane of GNB. We consider two models of the varying GNBs density distribution: (a) constant and (b) linear gradients of GNBs density (Fig. 1a). In addition, we discuss the intensity changes induced by the convolution of absorption correction with heterogeneous lattice rotations.

3.2. Laue diffraction from the gradient cell-wall dislocation structure with decaying dislocation density

Our analysis of cell-wall dislocation structure is based on the general kinematic treatment of X-ray scattering from crystals with dislocations and dislocation walls [5,17,18,20–22]. The precise shape of each Laue spot depends formally on the distribution of local orientations within the probed grain/subgrain volume. The intensity also depends on the incident beam spectral distribution near the Bragg energy of the reflection and the distribution of elastic deformation in the grain/subgrain. The initial spectral distribution can be described by $I_0(k)$, where ($k = |\boldsymbol{k}_0|$). The momentum transfer corresponding to a Bragg/Laue reflection G_{hkl} we define as, $k_{hkl} - k_0$, where ($|\boldsymbol{k}_0| = |\boldsymbol{k}_{hkl}| = k$) (Fig. 2). Here, k_0 is the incident wave vector and k_{hkl} is the scattered wave vector

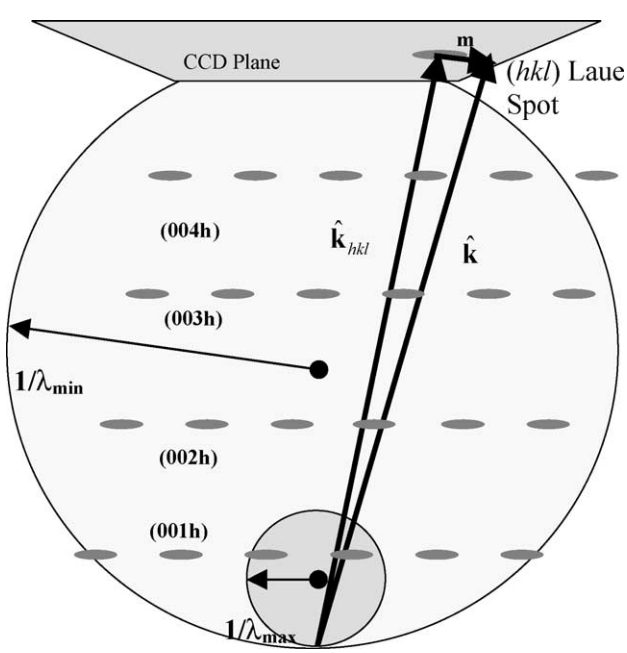

Fig. 2. Intensity of Laue image as a function of a misorientation vector $\boldsymbol{m}$. Laue spots (hkl), ($2h\,2k\,2l$) and ($3h\,3k\,3l$) give one spot at the CCD detector.

that satisfies the Bragg/Laue conditions. To analyze the white beam intensity distribution from a deformed grain, we introduce unit vectors in each direction of scattering $\hat{\boldsymbol{k}} = \boldsymbol{k}/|\boldsymbol{k}|$. Near a Bragg reflection we define a misorientation vector $\boldsymbol{m} = \hat{\boldsymbol{k}} - \hat{\boldsymbol{k}}_{hkl}$. The scattered intensity depends on the second rank dislocation density tensor ρ_{ik} via the displacement $\boldsymbol{u}_{\boldsymbol{k}}$ of each scattering cell from the equilibrium position $\boldsymbol{R}_k^0$.

$$I(\boldsymbol{Q}) = \left| \sum_k f_k \exp\left(i\,\boldsymbol{Q}(\boldsymbol{R}_k^0 + \boldsymbol{u}_k)\right) \right|^2. \tag{1}$$

Here f_k is the scattering factor from an individual atom k. The total displacement of i-th cell $\boldsymbol{u}_{\boldsymbol{i}}$ due to all GNBs is defined by the equation

$$\boldsymbol{u}_i = \sum_t c_t \boldsymbol{u}_{it}. \tag{2}$$

The intensity distribution of a crystal with GNBs may be written as follows [17,18,20,21]

$$I(\boldsymbol{q}) = f^2 \sum_{i,j} \mathrm{e}^{iq(R_i^0 - R_j^0)} \mathrm{e}^{-T}, \tag{3}$$

The correlation function T differs for different dislocation arrangements. The detailed analysis of the correlation functions for crystals with unpaired dislocations or dislocation walls can be found elsewhere [18]. After some kinds of plastic deformation crystals may form inhomogeneous distributions of geometrically necessary (unpaired) dislocations (GNDs) of one sign n^+ as well as geometrically necessary boundaries (Fig. 1). This causes not only local fluctuations in displacements from lattice sites, but also strongly correlated long-range rotations within the crystal, grain or subgrain. Such correlated deformation spreads the conditions for X-ray (or neutron) scattering transverse to the reciprocal space vector of each reflection and causes streaking of the Laue spot. Near an (hkl) Laue spot the diffracted intensity is strongly elongated in the ξ direction [17,18]. The streak direction, ξ, depends on the dislocation slip system orientation $\xi = \frac{\hat{\tau} \times \hat{G}}{|\hat{\tau} \times \hat{G}|}$.

3.3. Absorption correction

Eq. (3) describes the intensity distribution of Laue spots when the penetration depth is relatively small compared to the characteristic length of the lattice rotations along the beam; cases where the local orientation is roughly constant along the beam. In many measurements, however, this condition is invalid which alters the intensity distributions within the Laue streaks. For large penetration depths, Δ, it becomes important to take into account the attenuation of the intensity along the beam path both in and out of the crystal: $I = I_0\,\mathrm{e}^{-\mu x}$.

To illustrate the essential influence of absorption, we first describe the intensity distribution of an ideal crystal by delta-functions (neglecting the finite size of the crystal and other defects). The Laue image of a reference crystal before deformation consists of δ-functions in the symmetry positions of

the reciprocal space of the crystal. The measured Laue intensity at each point of a Laue pattern is an integral of $I(q)$ over the energy spectrum of the incident beam.

In the case of a large penetration depth we may approximately extend the integration to infinity and the diffracted Laue intensity profile can be written as,

$$I(\theta) = A \int_0^\infty \delta(\theta - \theta(x)) \mathrm{e}^{-\mu' x}\, \mathrm{d}x. \tag{4}$$

The integral Eq. (4) takes into account the absorption correction for an ideal reference crystal without dislocations. Below we show how it can qualitatively change the Laue intensity depending on the cell-wall structure arrangements.

3.4. Isotropic strain gradient distribution

We consider two simple models of cell-wall density gradients: Section 3.4, uniform; and Section 3.5, linear. Here, we assume that the cell interiors are free from dislocations and from long-range displacement fields. First we consider diffraction by a crystal with a constant density n^+ of geometrically necessary boundaries $\left(\frac{\partial n^+}{\partial x} = 0\right)$ forming tilt dislocations walls in the cell-wall structure. Each wall provides a local orientation shift Θ (Fig. 1a). The uniform distribution of GNBs creates a constant gradient of macroscopic lattice rotations (along the beam) with depth x:

$$\theta(x) = \theta_0 + \alpha n_0^+ \Theta x; \qquad \frac{\partial \theta}{\partial x} = \alpha \Theta n^+. \tag{5}$$

Here $\alpha = \alpha_\xi$ is the contrast factor along the streak.

The expression for the scattered intensity may be written explicitly as follows:

$$I(\theta) = A \int_0^\infty \delta\left(\theta - \theta_0 - \frac{\alpha \Theta x}{D^+}\right) \mathrm{e}^{-\mu' x}\, \mathrm{d}x;$$

$$I(\theta) = A \frac{D^+}{\alpha \Theta} \exp\left[-\frac{\mu' D^+ (\theta - \theta_0)}{\alpha \Theta}\right] \tag{6}$$

$I(\theta)$ has a single maximal value at $\theta = \theta_0$ formed by diffraction from the near-surface region and decreases exponentially with the deviation from this angle.

Simulations of the intensity distribution for uniform GNB density with an absorption correction are shown in Fig. 3. All simulations were performed using a microscopic description of the cell-wall structure and explicit distortion fields due to the dislocation arrangement. If we neglect the weakening of the intensity with depth ($\mu = 0$) the structure with constant dislocation GNBs density gives the "flat-top" shape of intensity profile along the Laue streak and for a symmetric (central) image the maximal value is in the center of the image (Fig. 3a). Absorption reduces the intensity arising from volumes deep within the sample resulting in an exponential tail to the Laue spot. The single maximum corresponds to the near surface region (Fig. 3b and c). This is in agreement with Eq. (6). The length of the streak increases with higher density of GNBs, and with lower absorption coefficient.

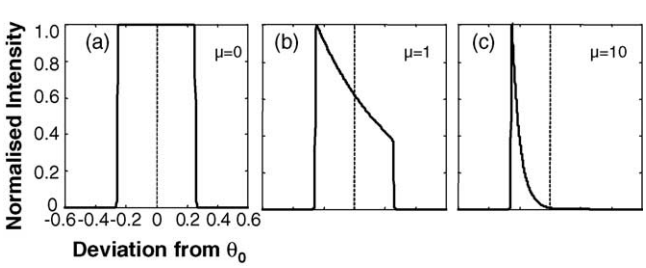

Fig. 3. Influence of absorption at constant GNBs density ($\beta = 0$) on the streak profile intensity distribution (a–c).

3.5. Linear decay of dislocation density with depth

Consider a linear decay of GNBs density with depth. This reasonable next approximation to actual dislocation arrangements can result in Laue streaking qualitatively distinct from that observed with a constant dislocation tensor field. Here, the dislocation tensor density is described by

$$n^+(x) = n_0^+(1 - \beta x) \quad \text{and} \quad \frac{\partial n^+}{\partial x} = -n_0^+ \beta \tag{7}$$

Here, n_0^+ is GNBs density near the crystal surface, β the decay coefficient of the GNBs density along the beam path in the sample. Lattice rotations and their gradient may for this case be written

$$\theta(x) = \theta_0 + \alpha n_0^+ \Theta x(1 - \beta x); \qquad \frac{\partial \theta}{\partial x} = \alpha n_0^+ \Theta (1 - 2\beta x) \tag{8}$$

For a linear decay of GNBs, the Laue spot intensity profile even for semi-infinite crystal can have two maxima of intensity due to the interplay between the decay of GNBs density and of scattering intensity with depth. An integration similar to Eq. (6) leads to the following expression for the intensity of the Laue streak

$$\boldsymbol{I} = \frac{\exp(-\mu \boldsymbol{x}_1(\theta))}{\frac{\partial \theta(\boldsymbol{x}_1(\theta))}{\partial \boldsymbol{x}}} + \frac{\exp(-\mu \boldsymbol{x}_2(\theta))}{\frac{\partial \theta(\boldsymbol{x}_2(\theta))}{\partial \boldsymbol{x}}} \tag{9}$$

The maxima correspond to the scattering from the depths:

$$x_{1,2} = \frac{\alpha n_0^+ \Theta \pm \sqrt{(\alpha n_0^+ \Theta)^2 - 4\alpha n_0^+ \Theta \beta (y - \theta_0)}}{2\alpha n_0^+ \Theta \beta} \tag{10}$$

Simulations show that the decay of GNBs density with depth redistributes the streak intensity (Fig. 4a–c). The most unusual shape of the streak is revealed when $\mu \sim \beta$ or $\mu < \beta$. Here, the interplay of the depth-dependent absorption with the dislocation density gradient results in a streak with maximal values at both sides (Fig. 4b). The first maximum corresponds to the scattering from a near surface region and the second is close to the scattering angle of the undistorted bulk crystal. The numerical simulations are in agreement with the continuum description (Eqs. (9) and (10)). A further decrease

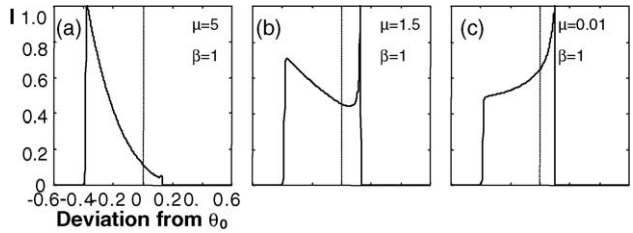

Fig. 4. Intensity profiles for linear gradient of GNBs ($\beta = 1$) and different ratio between β and μ (a–c).

of the μ/β ratio results in the appearance of a very strong maximum in the position close to undistorted bulk material and long weak tail (Fig. 4c). This Laue streak shape is observed in a number of experiments [16,17].

By comparing the two simple models above, we see that gradients in the dislocation tensor field can result in distinct Laue spot shapes with a peculiar intensity profile along the streak. When the unpaired dislocation density is small along the beam path (Fig. 4a) or the absorption large, then X-rays are scattered by planes with similar orientation. In cases with significant unpaired dislocation density (Fig. 4c) more interesting Laue spot shapes are created. By studying the shape of the Laue spot, DAXM methods can be extended to materials that are otherwise difficult to study.

4. Gradients of rotation in the Ni polycrystalline sample after uniaxial pulling

The theoretical approach described above was used to interpret the complicated Laue diffraction pattern and to obtain the parameters of the gradient cell-wall structure in a grain of a Ni polycrystal after in situ uniaxial pulling. Average grain size was ∼100 μm. The microbeam-Laue diffraction revealed pronounced streaking of the Laue spots after 15% strain. Laue images were reconstructed at different depths of a grain in the Ni polycrystalline sample. The orientation of the grain surface normal after deformation was almost parallel to $[\bar{2}\,3\,3]$ with loading direction approximately in $[1\,\bar{1}\,2]$ direction. The plastic response of the material in each grain can be described by the formation of cell wall structure in the material to relax the stress field induced during pulling.

Streaking of the Laue images reconstructed from μm-length volumes along the incident beam is observed up to 25 μm below the sample surface (Fig. 5). The total Laue pattern obtained from 30 μm consists of two sets of streaks. This is an indication that at least two regions with different slip systems and different strain gradient directions are present in the unresolved probed volume [16].

Differential aperture microscopy [16] demonstrated that in the near-surface region only one set of very-long streaks is present which is replaced by the second set of streaks at the depth of about 12–15 μm (Fig. 5b). Each set of streaks is related to a certain (predominant) dislocation slip system. Using the aforementioned theoretical analysis and fitting the experimental Laue pattern we determined the dislocation density tensor for both regions.

The analysis of the dislocation cell-wall substructure was performed in following steps:

- the orientation of eigenvectors and eigenvalues of the lattice curvature tensor were modeled from the streaks profiles of the experimental Laue pattern at each region;
- simulated Laue patterns using these eigenvectors were compared with the original experimental image;
- a least square fit was performed to find the predominant slip systems corresponding to the dislocation density tensor.

The Laue pattern simulated with the experimentally determined eigenvectors of the lattice curvature for a second region occupying the depth scale 15–30 μm is shown at Fig. 5c. Our analysis of the dislocation density tensor shows that the dislocation population, which is activated in this grain is mostly formed by edge dislocations with lines inclined approximately 45° to the loading direction.

All Laue spots have a highly asymmetric intensity distributions along the streak with a strong maximum at the end of the streak associated with the interior of the sample and with a long tail with gradually decreasing intensity. The in-

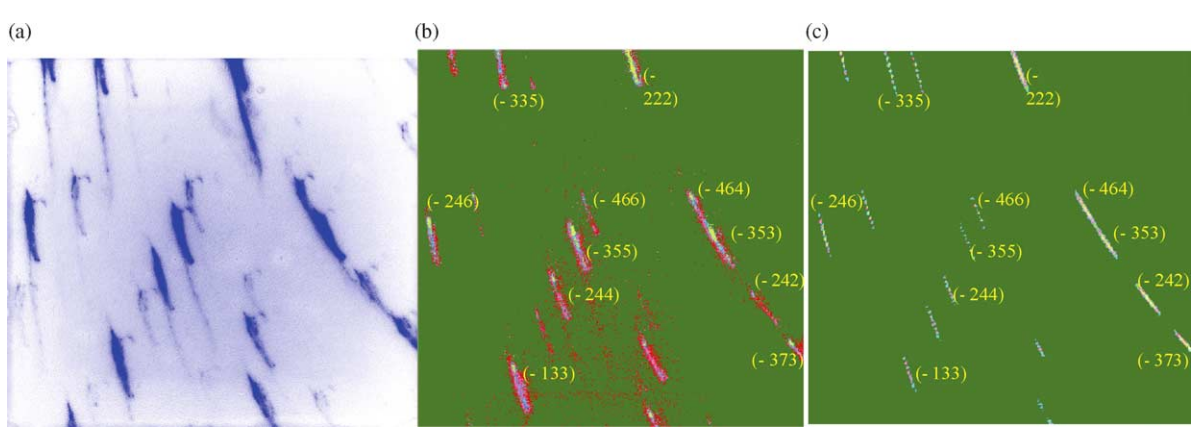

Fig. 5. Depth integrated (a) and depth resolved images (b and c) corresponding to the region within the depths 15–30 μm beneath the surface of the grain with a free surface in a Ni polycrystlal after uniaxial pulling: Experimental (b) and simulated (c) Laue images.

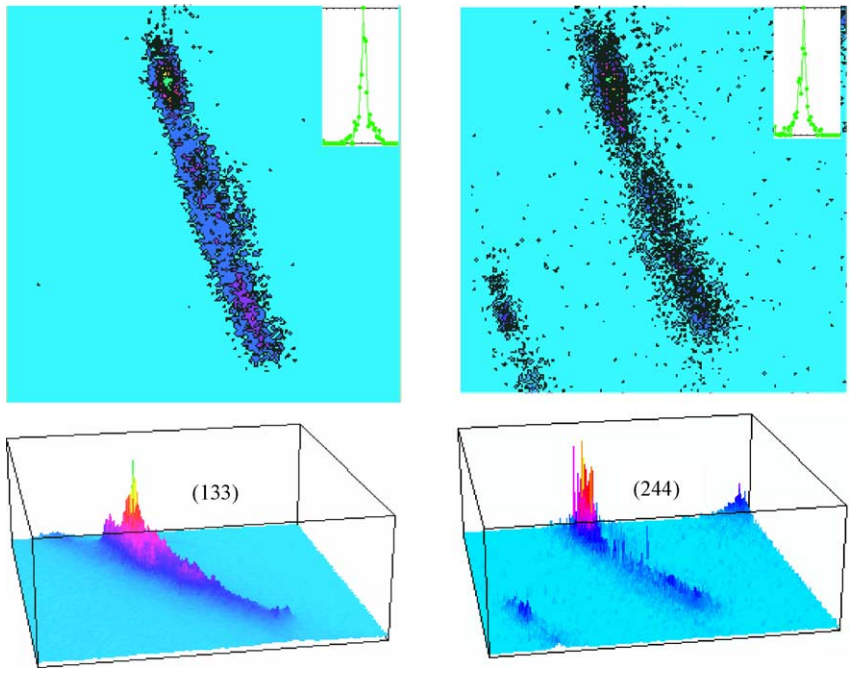

Fig. 6. Experimental contourmaps and 3D portraits of (1 3 3) and (2 4 4) Laue spots show asymmetric intensity distribution along the streak. Intensity profiles across the streak are shown at the inserts.

tensity maxima of all spots are located at the same end of the streak (Fig. 6). According to the previous discussion (Section 3.5) this particular asymmetry indicates a strong dislocation tensor gradient with depth. At depths beyond 30 μm, the Laue images became sharp and rotations in the grain were resolved with the differential-aperture technique. The results of the streak profile are in agreement with the results of the differential-aperture information.

The gradient in the cell-wall structure is understood to arise from the change in constraints near different boundaries of the analyzed grain and near the free surface. The number of constraints increases away from the surface toward the middle of the sample [23]. The observed gradient in the cell-wall structure has a length scale which differs from surface roughness, known to vary from 12 to 80 nm in similar experiments [24]. The observed gradients in GNBs with depth result in cumulative rotations and occupy regions with a much larger length scale of about ∼15 μm. They indicate the evolution of a hierarchical mesoscopic substructure. It evolves as a result of translational–rotational movement of the grain with free surface during pulling including both shear and rotation. Different structural levels are observed in this grain. The length scale at which the change of slip system orientation takes place (at the depth of about 12–15 μm) is comparable (approximately two times smaller) to the length scale of fractal dimensions found during tensile testing of Ni single crystal with AFM [24]. It is also in agreement with the length scale of mesoscopic slip sub-bands observed with EBSD during tension [25,26] and with earlier observations by Honeycombe [27] and Mughrabi et al. [28]. Earlier papers [25–27] demonstrate the inhomogeneities of plastic deformation based on the analysis of surface orientation maps. Extended analysis of 3D Laue diffraction measurements thus allow us to characterize inhomogeneities and orientation gradients in the cell-wall structure of materials.

5. Conclusions

- Inhomogeneities in the dislocation tensor as a function of depth in the grain of a Ni polycrystal after uniaxial pulling are observed.
- A decaying unpaired dislocation density with depth results in an asymmetric Laue streak profile with a strong intensity maximum arising from volumes deep in the sample and a long weak tail due to the near surface region.
- An analysis of the experimental intensity distribution along the streak profile allows the dislocation density gradient to be estimated due to the distinct intensity distribution for all Laue spots when corresponds to the case $\beta > \mu$ (Fig. 4c).
- Qualitatively the observed asymmetry of the intensity distribution along the streak profile indicates the presence of a significant dislocation density gradient leading to probed regions with high dislocation density and low dislocation density. This is definitely measurable within the penetration range of the ∼15–22 keV X-ray beam and both the large rotation field near the surface and the smaller gradient within the grain are probed simultaneously, as shown in Fig. 1a. This result is in agreement with our measurements of the grain rotation.
- The analysis of the dislocation density tensor shows that slip systems with dislocation lines inclined approximately 45° to the loading direction are activated first.

- A cumulative gradient in the cell-wall structure arrangement is observed for a "free surface" grain with the density of GNBs decaying into the depth of the grain.
- Several lamellar bands with predominant distinct slip system and effective strain gradients are formed within the first 40 μm depth of the grain. Change from one slip band to another takes place at ∼12–15 μm beneath the surface.
- Regions of cumulative rotations with a length scale of about 15 μm are observed.
- The results of microscopic description are in good agreement with predictions from the continuum approach.

Acknowledgements

Research is supported by the Director, Office of Science, Office of Basic Energy Sciences, U.S. Department of Energy, under Contract DE-AC05-00OR22725 with UT-Battelle. Experiments performed in part on Unicat Beamline 34-ID at the Advanced Photon Source, which is supported by the Department of Energy Office of Basic Energy Science.

References

[1] L. Marguilies, G. Winther, H.F. Poulsen, Science 291 (2001) 2392.
[2] H.F. Poulsen, D. Juul Jensen, G.B.M. Vaughan, MRS Bull. 29 (2004) 166.
[3] G.E. Ice, B.C. Larson, MRS Bull. 29 (2004) 170.
[4] B.C. Larson, W. Yang, G.E. Ice, J.D. Budai, J.Z. Tischler, Nature 415 (2002) 887.
[5] T. Ungar, H. Mughrabi, M. Wilkens, Acta Metall. 30 (1982) 1861.
[6] T. Ungar, H. Mughrabi, D. Ronnpagel, M. Wilkens, Acta Metall. 32 (1984) 333.
[7] F.J. Hamphreys, M. Hatherly, Recrystallization and Related Phenomena, Pergamon, 1999.
[8] D. Hughes, N. Hansen, Acta Mater. 48 (2000) 2985.
[9] D. Kuhlmann-Wilsdorf, N. Hansen, Scr. Metall. Mater. 25 (1991) 1557–1562.
[10] F.R.N. Nabarro, Theory of Crystal Dislocations, Dover Publications Inc., New York, 1987.
[11] D. Hughes, Proceedings of ReX'99 The Fourth International Conference on Recrystallization and Related Phenomena, The Japan Institute of Metals, Tsukuba City, Japan, 1999, p. 111.
[12] W. Pantleon, J. Mater. Res. 17 (9) (2002) 2433.
[13] N. Hansen, Metall. Mater. Trans. A 32A (2001) 2917.
[14] D.J. Jensen, W. Pantleon, in: A. Khan (Ed.), Proceedings of Plasticity'03: The Tenth International Symposium on Plasticity and its Current Applications, 490, 2003.
[15] D.A. Hughes, N. Hansen, D.J. Bammann, Scr. Mater. 48 (2003) 147.
[16] G.E. Ice, R.I. Barabash, J.W.L. Pang, Multiscale phenomena in materials Experiments and Modeling Related to Mechanical Behavior, in: M. Zbib, D. Lassila, L. Levine, K. Hemker (Eds.), Material Research Society, Warrendale, Penn., 779, W6.6.1, 2003.
[17] R.I. Barabash, G.E. Ice, B.C. Larson, G.M. Pharr, K.S. Chung, W. Yang, APL 79 (2001) 4.
[18] R.I. Barabash, G.E. Ice, F. Walker, J. Appl. Phys. 93 (3) (2003) 1457.
[19] G. Saada, E. Bouchaud, Acta Metal. Mater. 41 (1993) 2173.
[20] M. Krivoglaz, X-ray and Neutron Diffraction in Nonideal Crystals, Springer, Berlin, 1996.
[21] M. Wilkens, Phys. Stat. Sol. A. 2, 359, in: J.A. Simmons, R. de Wit, R. Bullough (Eds.), Fundamental Aspects of Dislocation Theory II, p.1195, Natl. Bur. Stand. Special Publication, Washington, 317, II, K1, 1970.
[22] R. Thomson, L. Levine, Acta Cryst. A53 (1997) 590.
[23] W.F. Hosford, The Mechanics of Crystals and Textured Polycrystals, Oxford Engineering Science Series, Oxford University Press, 1993.
[24] O. Maiβner, J. Schreiber, A. Schwab, Appl. Phys. A 66 (1998) S1113.
[25] T. Okada, X. Huang, K. Kashihara, F. Inoko, J.A. Wert, Acta Mater. 51 (2003) 1827.
[26] J.A. Wert, X. Huang, F. Inoko, Proc. R. Soc. Lond. **A** 453 (2003) 85.
[27] R.K.W. Honeycombe, J. Inst. Met. 80 (1951) 45.
[28] H. Mughrabi, T. Ungar, M. Wilkens, Scripta Metall. 17 (1983) 797.